Construction and Building Materials 262 (2020) 120075

Contents lists available at ScienceDirect

Construction and Building Materials

journal homepage: www.elsevier.com/locate/conbuildmat

X-ray CT based clogging analyses of pervious concrete pile by vibrating-sinking tube method

Xinzhuang Cui [a], Xiaoning Zhang [a], Jipeng Wang [a,*], Jiong Zhang [a], Hui Qi [b], Jun Li [a]

[a] School of Civil Engineering, Shandong University, Jinan 250061, PR China
[b] Qilu Transportation Development Group, Jinan 250101, PR China

HIGHLIGHTS

- A simulation installation system of the pervious concrete pile by vibrating-sinking tube method was developed.
- Clogging depth and porosity of pervious concrete pile were studied based on X-ray CT imaging.
- The effect of geotextile on pervious concrete pile anti-clogging was evaluated.
- The evolution of excess pore water pressure in the pervious concrete pile composite foundation was analyzed.

ARTICLE INFO

Article history:
Received 2 March 2020
Received in revised form 22 June 2020
Accepted 24 June 2020
Available online 9 July 2020

Keywords:
Pervious concrete pile
Vibrating-sinking tube
Model test
X-ray CT
Clogging

ABSTRACT

Pervious concrete piles (PCP) have high permeability and strength. During installation by vibrating-sinking tube construction, liquified soil migrates into PCP, leading to clogging. To study PCP clogging, model tests and X-ray computed tomography analyses were carried out. The clogging depth, porosity, and excess pore water pressure dissipation were characterized. The effect of geotextile on PCP anti-clogging was evaluated. The results show an increase in target porosity and sampling depth significantly increased the PCP clogging depth. A preliminary model was proposed to evaluate the clogging of PCP. The results show that clogging can be solved by surrounding PCP with geotextile.

1. Introduction

In recent years, the composite foundation technologies as a widely applied technology can be used to enhance the bearing capacity of the foundation and to reduce settlement and liquefaction potential of ground [1,2]. The vertical reinforcements of the composite foundation are divided into a granular pile, flexible pile, and rigid pile. The granular pile can accelerate the rate of consolidation and reduce the liquefaction potential of sand or silt ground [3–6]. However, the granular pile has relatively low stiffness and strength, which is also greatly influenced by the confining pressure of the surrounding soil [7]. Therefore, when the granular pile is applied to soft clay, organic, or peat soil, the shallow part of this pile is prone to expansion failure, and thus the bearing capacity of the ground has little improvement. While the rigid piles such as low-grade concrete pile and cement fly-ash grave pile have overcome the weak bonding problem of granular piles [8–11], but with poor permeability, resulting in slow consolidation rate of ground.

Based on the above, an innovative ground improvement method using pervious concrete pile (PCP) was proposed by Suleiman et al [12]. Since pervious concrete (also referred to as porous concrete) is a mixture of Portland cement, gap graded aggregate, and water with or without a small amount of fine aggregate, there is a large number of connective pores within the aggregate skeleton. Generally, the porosity of pervious concrete is between 15% and 45% and has good permeability [13–16]. With the good permeability, the pervious concrete can also provide a certain compressive strength [17–19]. Therefore, PCP has advantages of both granular pile and rigid pile [20]. The fast drainage capacity can accelerate excess pore water pressure dissipation, subsoil consolidation, and post-construction settlement of the upper construction, such as road embankment. However, when installing the PCP, silty sand or silt liquefaction often occurs. These silts facilitate

* Corresponding author.
E-mail addresses: cuixz@sdu.edu.cn (X. Cui), sdjtuzxn@163.com (X. Zhang), ji-peng.wang@sdu.edu.cn (J. Wang), jiongzhang@sdu.edu.cn (J. Zhang), 1016913282@qq.com (H. Qi), forzaapis@126.com (J. Li).

https://doi.org/10.1016/j.conbuildmat.2020.120075
0950-0618/

the clogging of PCP by migrating fine soil particles into the fresh concrete pile. In the literature, the performance of the PCP composite foundation was studied using instrumented model laboratory tests [21,22], and the clogging of pervious concrete was studied using numerical simulations [23,24] and small model laboratory test [25]. There is no relevant research on PCP clogging caused by the vibrating-sinking tube method, and no relevant research on PCP anti-clogging method.

In addition, image processing technology, CT technology, and X-Ray technique are utilized in the microscopic study of porous materials. Stereological and morphological methods are used to extract relevant pore structure features of pervious concretes from planar images [26,27]. A few studies also analysed the permeability performance of pervious concrete using CT and reconstruction methods. A computational procedure is employed to predict the permeability of different pervious concrete mixtures from 3D material structures reconstructed from the original material [28]. Based on X-Ray Technique, Kuang [29] studied the permeable pavement pore-structure parameters using the modified Kozeny-Carman model. Chung [30] used X-ray CT images to obtain the spatial distribution of the voids, used low-order probability functions to reconstruct porous concrete specimens, and simulated the hydraulic conductivity of reconstructed specimens. Xu [31] studied the internal structure evolution within asphalt mixtures under freeze–thaw cycles using X-ray CT images.

To the best of our knowledge, the clogging of PCP due to the vibrating-sinking tube construction has not been given full attention yet, although the issue of clogging has been questioned since PCP was proposed. Therefore, this study focus on the experimental characterization of PCP clogging caused by soil liquefaction during the vibrating-sinking tube construction period. Here, a physical modeling system is developed to study the clogging of PCP under vibrating-sinking tube construction. Using this new set-up and CT, a series of laboratory simulation tests are conducted to demonstrate the effects of vibrating-sinking tube construction on the clogging of PCP and the anti-clogging performance of geotextile.

2. Model test

2.1. Test system

When the pore of PCP is clogged, the permeability is bound to decrease. In this study, an installation system of PCP by vibrating-sinking tube is developed, as shown in Fig. 1. The modeling system is divided into a model test box, vibrating-sinking tube installation equipment, pore water pressure sensor, and data acquisition equipment. Its functions are as follows: (1) to simulate the installation process of PCP; (2) to simulate the liquefaction and migration of fine soil during the installation of the vibrating-sinking tube; and (3) to continuously record the excess pore water pressure during and after the installation of PCP.

The length, width, and height of the composite foundation model test box were 2000 mm, 1000 mm, and 1050 mm respectively. The length, width, and height of the vibrating-sinking tube simulated construction system was 3600 mm, 2000 mm, and 3300 mm respectively.

2.2. Model test material

2.2.1. Pervious concrete

Pervious concrete mixtures were prepared using ordinary Portland cement and coarse aggregates. The aggregates are composed of limestone rubble with particle sizes ranging from 4.75 mm to 9.5 mm (single-size). The mineralogical composition obtained by XRD is 93% calcite, 3.7% quartz, and 3.3% dolomite for the limestone. The gradation curve of the aggregate is shown in Fig. 2. The physical properties of this aggregate are presented in Table 1.

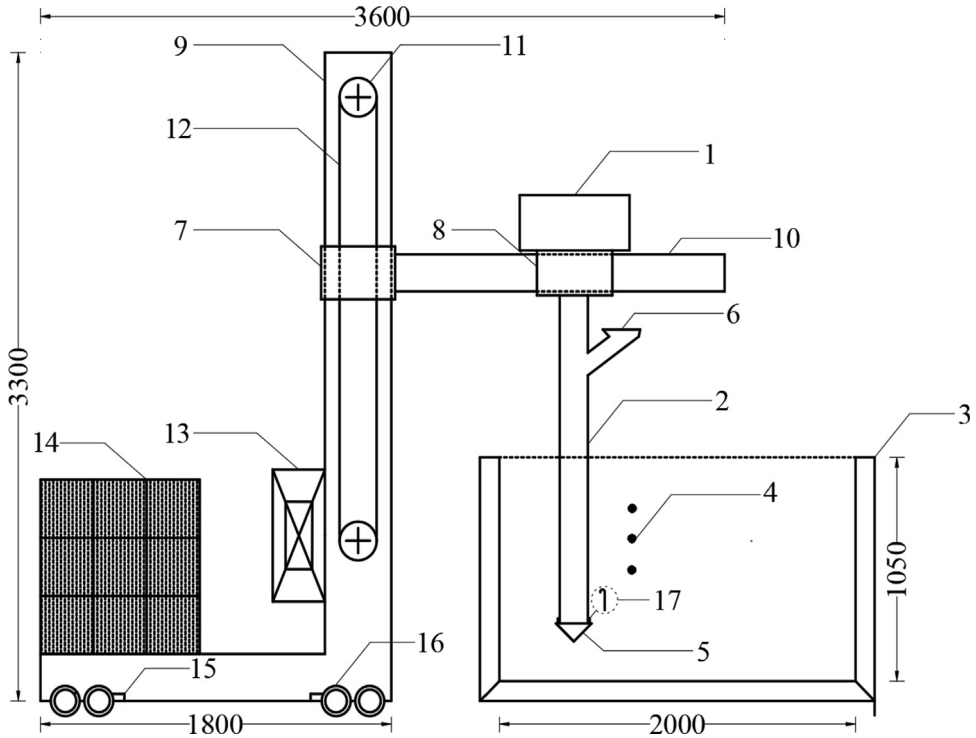

Fig. 1. Vibrating-sinking tube construction simulation test system 1. Vibration table; 2. Tube; 3. Model box; 4. Pore water pressure sensor; 5. Concrete pile tip; 6. Feeding inlet; 7. Vertical sliding table; 8. Horizontal sliding table; 9. Vertical steel frame; 10. Horizontal steel frame; 11.Roller; 12. Fairlead; 13. Lift engine; 14. Counterweight iron; 15. Wheel lock; 16. Wheel; 17. An iron hook for securing geotextiles.

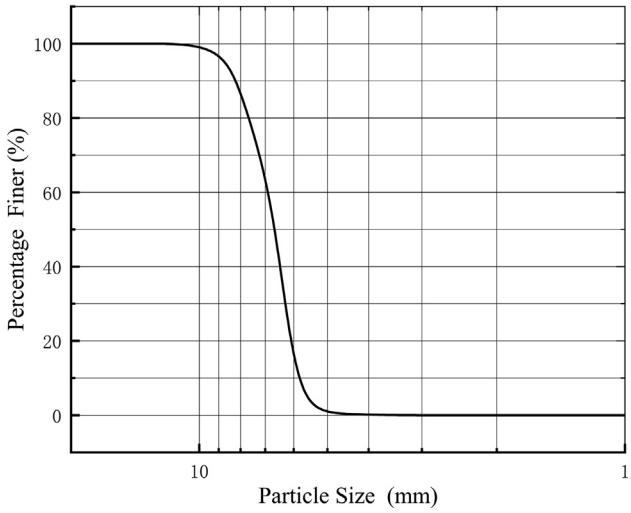

Fig. 2. Gradation curve of aggregate.

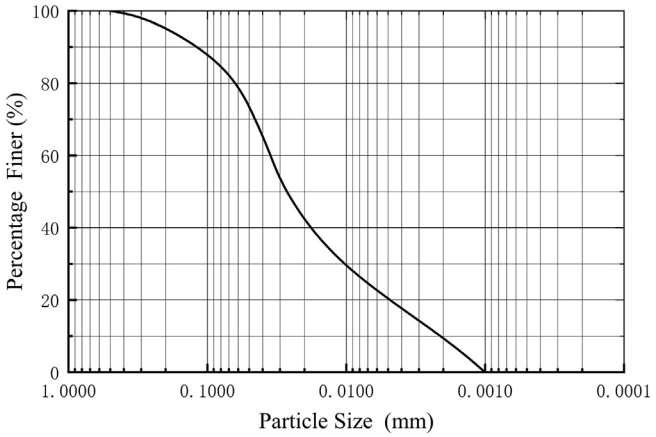

Fig. 3. Gradation curve of soil.

Four target porosities (10%, 15%, 20%, 25%) were designed for the pervious concrete in this work. And the mix design method was originally proposed by Cui et al [32]. The mix proportions of pervious concrete are listed in Table 2. Moreover, it is worth mentioning that the sulphamate series superplasticizer is chosen to decrease water usage, thereby ensuring good fluidity of the pervious concretes.

2.2.2. Soil

The foundation soil comes from the Yellow River Delta in Shandong Province and is low liquid limit silt. The non-clay mineral content is 85 ~ 90%, mainly including quartz, feldspar, carbonate mineral, and trace hornblende. The clay mineral content is 10 ~ 15%, mainly illite, montmorillonite, a small amount of kaolinite and chlorite. Notably, illite is about 75% of the total clay minerals. The physicochemical properties of the tested silt are shown in Table 3. According to Hideaki et al [33], the gradation curve of soil used is in the range of liquefiable soil, as shown in Fig. 3. The coefficient of uniformity C_u is 9.72, and the coefficient of curvature is 1.40, so it is not piping soil.

2.2.3. Non-woven geotextile

Non-woven geotextile is to arrange the fibers randomly to form a network structure and then make a plain fabric. The non-woven geotextile has no directionality in terms of strength, and the mesh structure formed by the amorphous fiber has flexibility and mobility, so the mesh is unlikely to clog. The parameters of non-woven geotextile are presented in Table 4.

3. Test procedure and scheme

3.1. Test cases

As shown in Table 5, Fig. 4, and Fig. 6, eight test cases were proposed: O-1, O-2, O-3, and O-4 are ordinary pervious concrete piles (O-PCP); and AC-1, AC-2, AC-3, AC-4 are anti-clogging pervious concrete piles (AC-PCP) based on geotextile. Specifically, four porosities (10%, 15%, 20%, and 25%) and four sampling depths (20 cm, 40 cm, 60 cm, and 80 cm) were chosen, respectively. For each case, three samples were tested to ensure the scientific nature and accuracy of the test results.

As shown in Table 6 and Fig. 4, to accurately analyse the pore water pressure of the eight test cases. Three pore water pressure burial depths (25 cm, 50 cm, and 75 cm) were used. The pore water

Table 1
Physical properties of aggregates in pervious concretes.

Size (mm)	Apparent density (g/cm^3)	Stacking density (g/cm^3)	Porosity (%)	Crushed percentage (%)
4.75–9.5	2.665	1.655	37.89	8.6

Table 2
Mix proportions of per cubic meter of pervious concrete.

Target porosity (%)	Cement (kg/m^3)	Water (kg/m^3)	Aggregate (kg/m^3)	Superplasticizer dosage (%)
10	417.8	160.4	1587.6	0.8
15	396.3	134.8		
20	320.9	109.1		
25	245.4	83.4		

Table 3
Physicochemical properties of silt tested.

Moisture content(ω %)	Initial void ratio(e %)	Intact density(g·cm^3)	Liquidlimit(ω_L %)	Plasticity limit(ω_P %)	Plasticity index(I_P %)	pH
25.5	0.71	1.96	27	20	7	7.4 ~ 8.1

Table 4
Non-woven geotextile parameters.

Thickness(mm)	Breaking strength(kN/m)	Elongation at break (%)	Effective aperture (mm)	Hydraulic conductivity(cm/s)
1.7	6.5	30	0.07 ~ 0.2	1.0 ~ 9.9×(10^{-1} ~ 10^{-3})

Table 5
Test cases of PCP clogging.

O-PCP Case	Test samples	Target Porosity P (%)	Sampling depth H (cm)	AC-PCP Case	Test samples	Target Porosity P (%)	Sampling depth H' (cm)
O-1	A	10	20	AC-1	A	10	20
	B	10	40		B	10	40
	C	10	60		C	10	60
	D	10	80		D	10	80
O-2	A	15	20	AC-2	A	15	20
	B	15	40		B	15	40
	C	15	60		C	15	60
	D	15	80		D	15	80
O-3	A	20	20	AC-3	A	20	20
	B	20	40		B	20	40
	C	20	60		C	20	60
	D	20	80		D	20	80
O-4	A	25	20	AC-4	A	25	20
	B	25	40		B	25	40
	C	25	60		C	25	60
	D	25	80		D	25	80

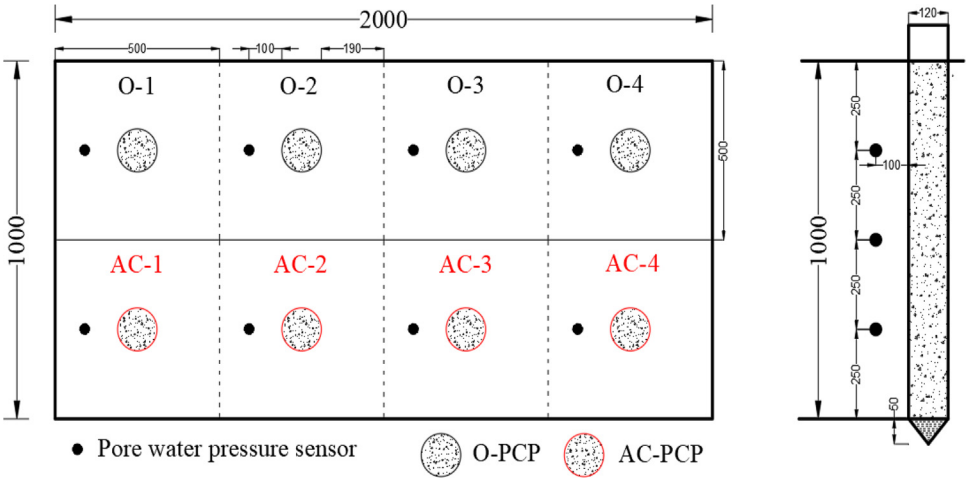

Fig. 4. Layout diagram of PCP and pore water pressure sensor.

Table 6
Test cases of pore water pressure.

O-PCP Case	Pore water pressure sensor	Target porosity P (%)	Burial depth of sensor h (cm)	AC-PCP Case	Pore water pressure sensor	Target porosity P (%)	Burial depth of sensor h' (cm)
O-1	1	10	25	AC-1	1	10	25
	2	10	50		2	10	50
	3	10	75		3	10	75
O-2	1	15	25	AC-2	1	15	25
	2	15	50		2	15	50
	3	15	75		3	15	75
O-3	1	20	25	AC-3	1	20	25
	2	20	50		2	20	50
	3	20	75		3	20	75
O-4	1	25	25	AC-4	1	25	25
	2	25	50		2	25	50
	3	25	75		3	25	75

pressure sensors were horizontally arranged 100 mm away from the pile.

3.2. Installation of piles

The vibrating-sinking tube method is used to install PCP, and the construction process and model piles are shown in Fig. 5. In the PCP installation process, when the tube tip attains to the designed depth, the calculated volume of pervious concrete was poured into the tube through the feeding inlet. Starting the motor, the tube should be kept vibrating for 10 s. And then the tube is gradually withdrawn with continuous vibration. The withdrawing speed was controlled between 2.2 and 2.5 m/min. If sludge is discovered during withdrawal, the withdrawal speed needs to be adjusted. Here, it should be noted that during the installation of AC-PCP, the geotextiles should be made into a cylinder shape in advance and fixed on the outside of the vibrating-sinking tube. During the installation, the geotextile tube sinks into the soil with the vibration tube.

3.3. Test procedures

3.3.1. PCP clogging test

Using a model system, industrial CT, and 3D reconstruction, the clogging tests of PCP are carried out according to the following procedures:

Step 1: The O-PCP and AC-PCP model piles were obtained through the model test system. (Fig. 5(b)).

Step 2: The standard sample (size: length × width × height = 60 mm × 35 mm × 40 mm) is obtained by cutting in the radial direction. To ensure the resolution of the CT scan and meet the requirements of the CT instrument on the size of the sample, the model pile needs to be processed. In this test, the most representative part in the middle of the model pile was selected for the CT scan. In order to obtain the pore-clogging caused in the radial direction, samples were cut along the radial direction. The sample extraction process is shown in Fig. 6.

Step 3: The standard samples were scanned using an Xradia 510 Versa microscope. (Fig. 7).

Step 4: The three-dimensional (3D) reconstruction software is used for visualization and numerical processing to analyse the clogging of model piles.

3.3.2. Pore water pressure test

In this study, a miniature pore water pressure sensor with a small volume and high sensitivity were used. The data acquisition system uses a high-precision 24-bit A/D converter and a high-performance ARM processor. It has good measurement accuracy, good stability, and strong anti-interference ability. The pore water pressure data were collected in real-time during and after the test.

4. Test results and analyses

4.1. Clogging depth

4.1.1. Calculation of PCP clogging depth

The calculation of the PCP clogging depth is carried out according to the following procedures:

Step 1: Multi-section test data was obtained by the CT scan.

Step 2: Threshold segmentation based on multi-section test data. For this test, the internal structure of pervious concrete is composed of aggregate, cement, porosity, and clogging the soil. Because the density of each component is different, the brightness in the reconstructed image will vary. The higher the density of the material, the higher the brightness, so the gray value of each component will be in a certain range. The threshold segmentation of the CT image is shown in Fig. 8. The blue represents clogging soil, red represents aggregate and light blue represents porosity.

Step 3: Calculation of clogging depth based on CT imaging. Firstly, the 300th, 500th, and 800th slices (Fig. 9(a)) are taken ver-

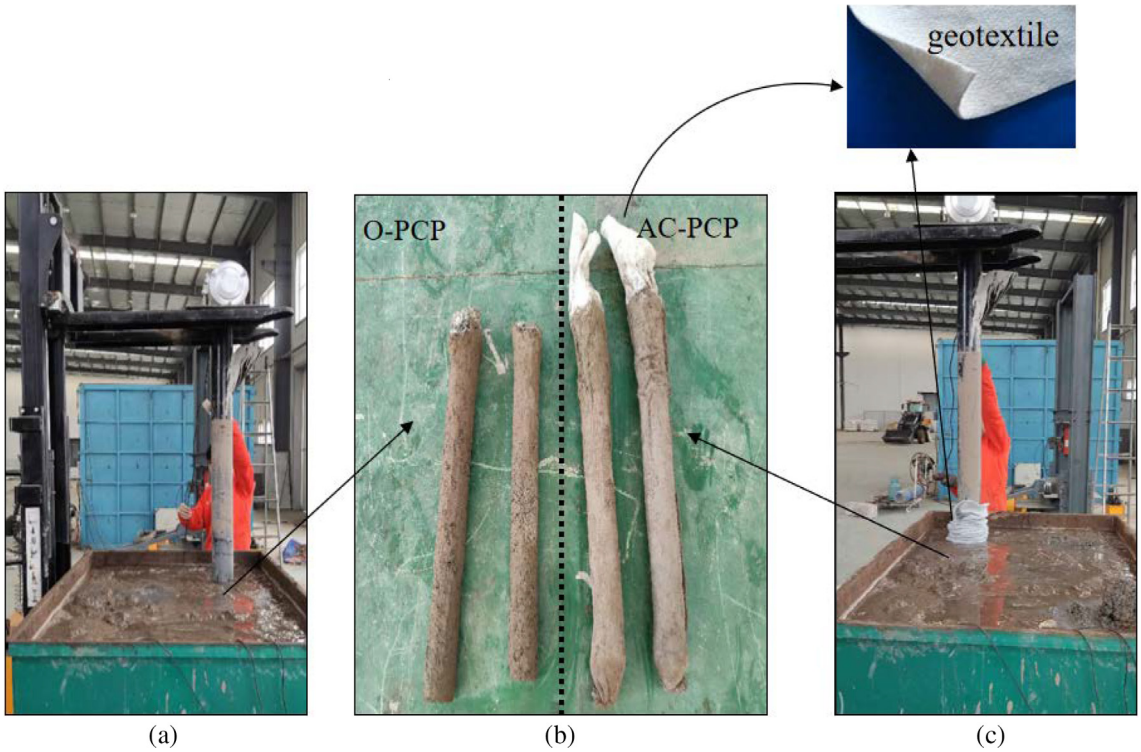

Fig. 5. The installation of PCP. (a) Installation of O-PCP; (b) The O-PCP and AC-PCP model piles; (c) Installation of AC-PCP.

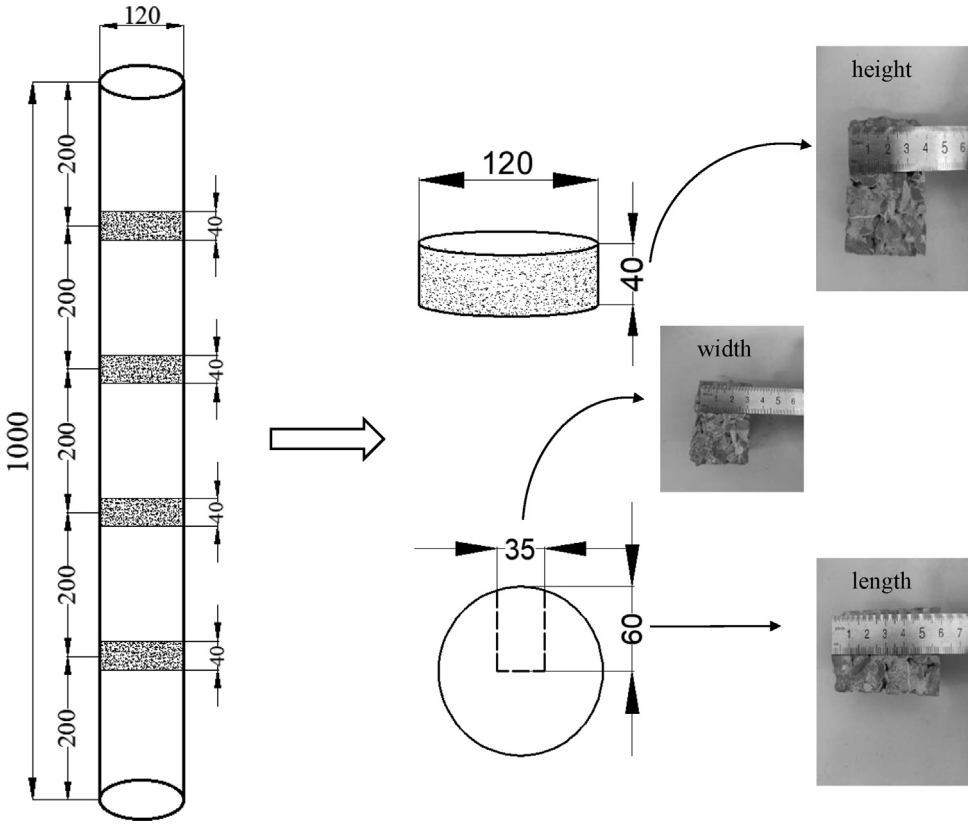

Fig. 6. The sample extraction process.

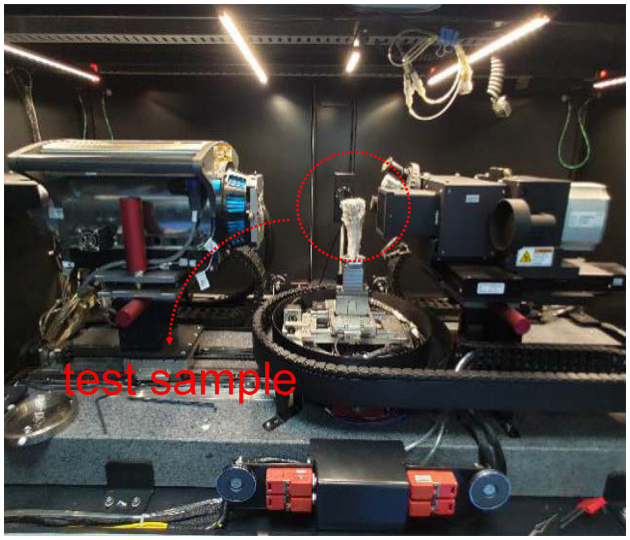

Fig. 7. The X-ray scan set-up.

tically from the samples (O-4-C case as an example). From Fig. 9(b), it can be seen that the clogging depth of soil at different positions is relatively uniform. Then, the 1000th, 900th, and 600th horizontal slices (Fig. 10(a)) are taken. From Fig. 10(b), it can be seen that with the increase of depth, the volume of clogging soil in the section gradually decreases, and the clogging soil disappears in the 600th slice, so it can be judged that this position is the deepest position of the clogging soil.

The calculation formula for the clogging depth of the sample, as indicated in Eq. (1).

$$D = \frac{l_x}{l} L \tag{1}$$

where D is the sample clogging depth (mm), l_x is the number of slices corresponding to the sample deepest clogging position, l is the total number of horizontal slices, L is the sample length (mm).

4.1.2. PCP clogging depth analyses

The variation curves of the D with porosity and sampling depth are shown in Fig. 11. It is evident that AC-PCP has almost no clogging, and parts of the soil entered to the pile surface due to a small amount of soil during geotextile installation. O-PCP has different degrees of clogging under different target porosities. With the increase in the target porosity and sampling depth, clogging depth increases nonlinearly. When the target porosity exceeds 15%, the increase of the clogging depth is obvious. When the target porosity reaches 25%, the clogging depth reaches 39.78 mm.

4.1.3. Model of PCP clogging depth

We use the ratio of clogging depth to the radius of the pile after construction to present the normalized PCP clogging depth (*NPC*), as indicated in Eq. (2). The variation curves of *NPC* with porosity are shown in Fig. 12.

$$NPC = \frac{D}{R} \tag{2}$$

where *NPC* = normalized PCP clogging depth, D = clogging depth, R = PCP radius.

It can be seen that all the curves in Fig. 12 demonstrated significant similarities. Therefore, as shown in Fig. 13, a ratio can be defined as the *NPC* divided by the NPC_{25} to eliminate the effects of sampling depth H, where the NPC_{25} is the normalized clogging depth corresponding to the porosity of 25%. It is shown in Fig. 13 that the variation of NPC/NPC_{25} is independent of the sampling

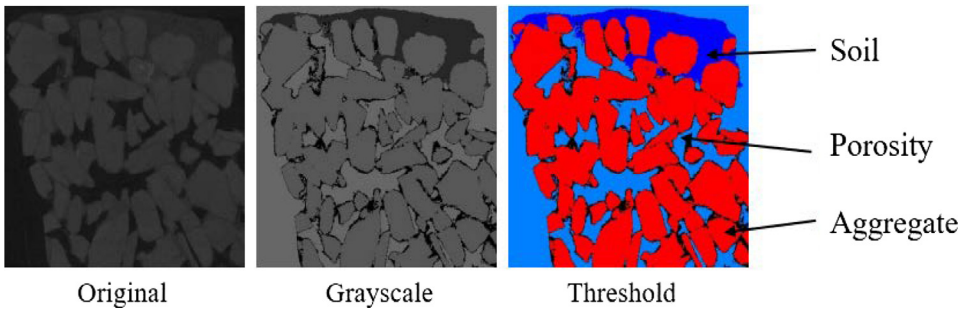

Fig. 8. Threshold segmentation of CT image.

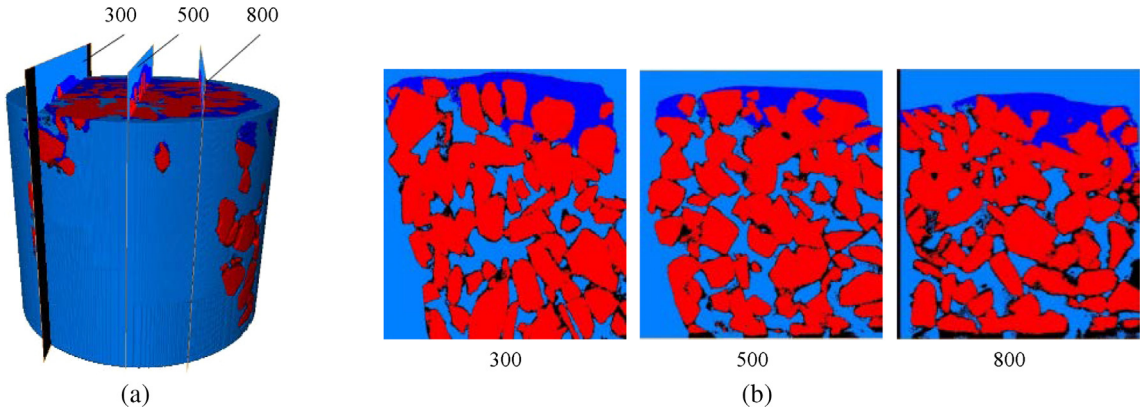

Fig. 9. Vertical slice of sample.

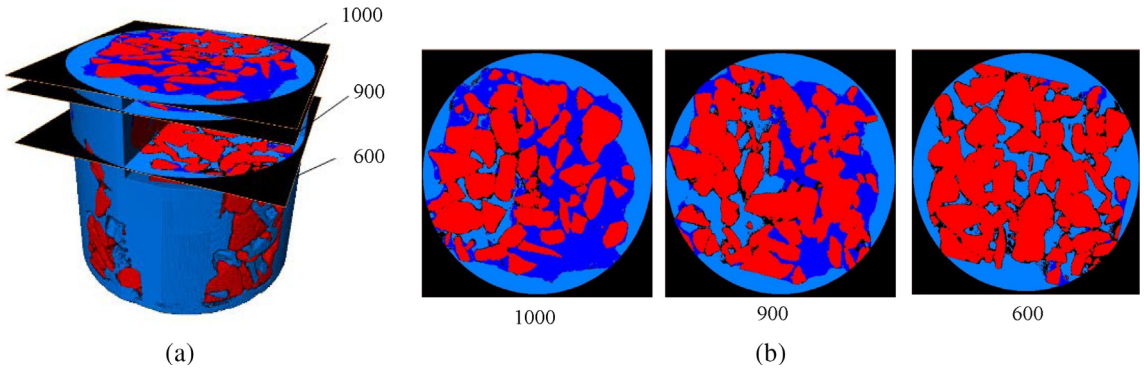

Fig. 10. Horizontal slice of sample.

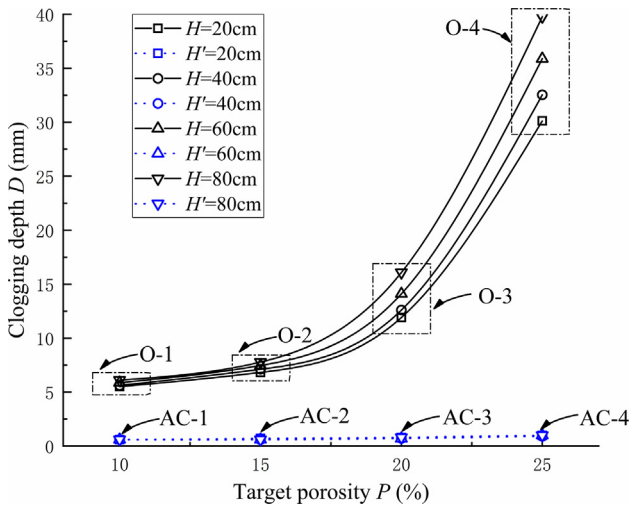

Fig. 11. Variation curves of the D with porosity and sampling depth.

depth H. Moreover, the variation trend can be well fitted via the following exponential function, as indicated in Eq. (3).

$$\frac{NPC}{NPC_{25}} = 0.00963\exp(P/5.25) - 0.01526P + 0.26709(R^2 = 0.99) \quad (3)$$

where P is the target porosity and NPC_{25} is the normalized clogging depth of the O-PCP when the porosity is 25%.

In Eq. (3), NPC_{25} is related to sampling depth H, and the variation trend of NPC_{25} with sampling depth is demonstrated in Fig. 14. It can be seen that NPC_{25} increases linearly with the sampling depth. Using the linear regression analysis, the relationship between NPC_{25} and the sampling depth can be established, as indicated in Eq. (4).

$$NPC_{25} = 0.00269H + 0.44167(20cm \le H \le 80cm)(R^2 = 0.99) \quad (4)$$

where NPC_{25} is the normalized clogging depth of O-PCP when the porosity is 25%; H is the sampling depth and R is the correlation coefficient.

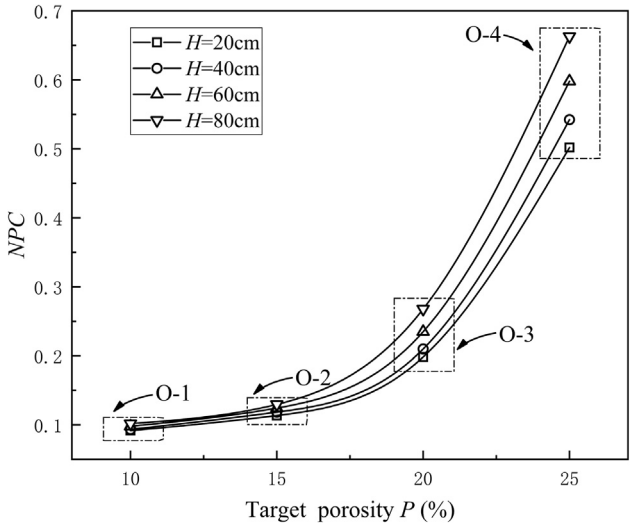

Fig. 12. Variation curves of the *NPC* with porosity.

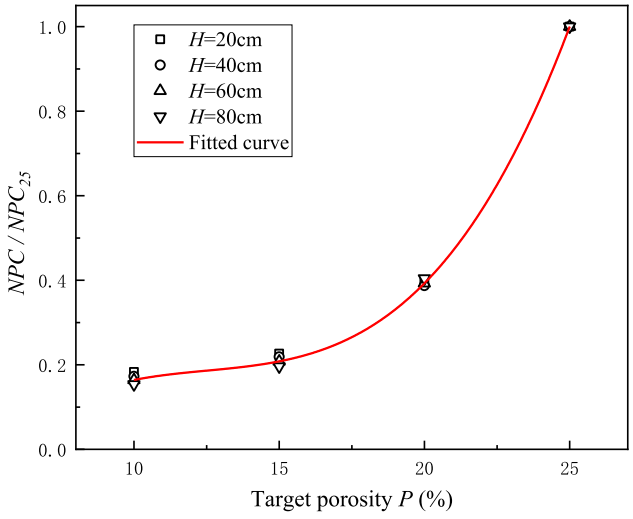

Fig. 13. Variation curve of the NPC/NPC_{25} with porosity.

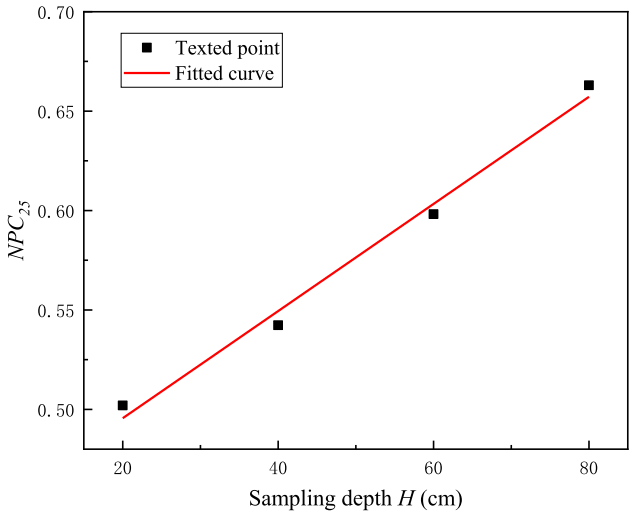

Fig. 14. Variation curve of the NPC_{25} with sampling depth.

Form Eq. (3) and Eq. (4), a nonlinear model of the normalized clogging depth can be proposed within the sampling depth range of 20 cm to 80 cm, as indicated in Eq. (5).

$$NPC = [(0.00963\exp(P/5.25) - 0.01526P + 0.26709)] \times (0.00269H + 0.44167) \quad (5)$$

The Eq. (5) is a uniform model, and it can be seen that the independent variables in Eq. (5) include both porosity and sampling depth. This means that this uniform model can reflect the effects of porosity and sampling depth on the normalized clogging of PCP. And as shown in Fig. 15, the fitted values have a high consistency with the measured values.

4.2. PCP porosity

The porosity calculation of AC-PCP and O-PCP before and after clogging is as follows. Firstly, the overall threshold of the sample is obtained, and the pores are obtained by threshold segmentation. Subsequently, the porosity is calculated by the volume fraction calculation module, and the 3D porosity is obtained. However, this method for the analysis of porosity has little error. In the process of threshold segmentation, air on both sides of the sample is considered as pores, leading to a larger porosity computation. To eliminate the influence of this factor, we derive an accurate porosity calculation formula, as indicated in Eq. (6).

$$P_f = \frac{P' - P_o' - P_s'}{1 - P_o'}(a)P_s = \frac{P_s'}{1 - P_o'}(b)P_a = P_f + P_s(c) \quad (6)$$

where P_f is the final porosity after clogging, P_s is the ratio of the clogging soil volume to the pervious concrete volume, P_a (actual initial porosity) is the ratio of pore volume to pervious concrete volume, P' is the ratio of pore volume to the sum of pervious concrete volume and air volume, P_o' is the ratio of air volume to the sum of pervious concrete and air volume, and P_s' is the ratio of the clogging soil volume to the sum of pervious concrete volume and air volume.

The final porosity after clogging, actual initial porosity, and target porosity are indicated in Table 7. The relationship between the target porosity and the porosity after clogging is shown in Fig. 16.

Fig. 16 shows, almost all the actual initial porosity is slightly higher than the target porosity, which shows that the PCP mix ratio design and installation method adopted in this paper are accurate

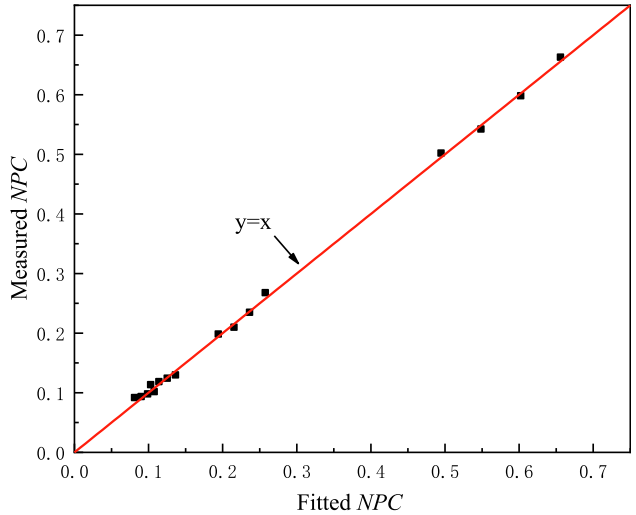

Fig. 15. The relationship between measured and fitted *NPC*.

Table 7
Porosity of PCP.

O-PCP Case		Target porosity$P$ (%)	Actual initial porosityP_a (%)	Porosity after cloggingP_f (%)	AC-PCPCase		Target porosity$P$ (%)	Actual initial porosityP_a (%)	Porosity after cloggingP_f (%)
O-1	A	10	11.04	10.53	AC-1	A	10	11.05	11.04
	B	10	11.22	10.68		B	10	11.23	11.17
	C	10	11.20	10.61		C	10	11.30	11.19
	D	10	11.32	10.70		D	10	11.22	11.02
O-2	A	15	15.11	14.45	AC-2	A	15	15.54	15.14
	B	15	15.22	14.33		B	15	15.43	15.17
	C	15	15.26	14.38		C	15	15.30	15.18
	D	15	15.24	14.21		D	15	15.34	15.18
O-3	A	20	19.93	18.33	AC-3	A	20	20.22	19.98
	B	20	20.13	18.20		B	20	20.23	20.08
	C	20	20.21	17.72		C	20	20.32	19.97
	D	20	20.17	17.11		D	20	20.34	20.12
O-4	A	25	24.92	22.83	AC-4	A	25	25.31	24.87
	B	25	25.01	21.45		B	25	25.21	25.04
	C	25	24.94	20.13		C	25	25.30	24.74
	D	25	24.87	18.81		D	25	25.21	25.11

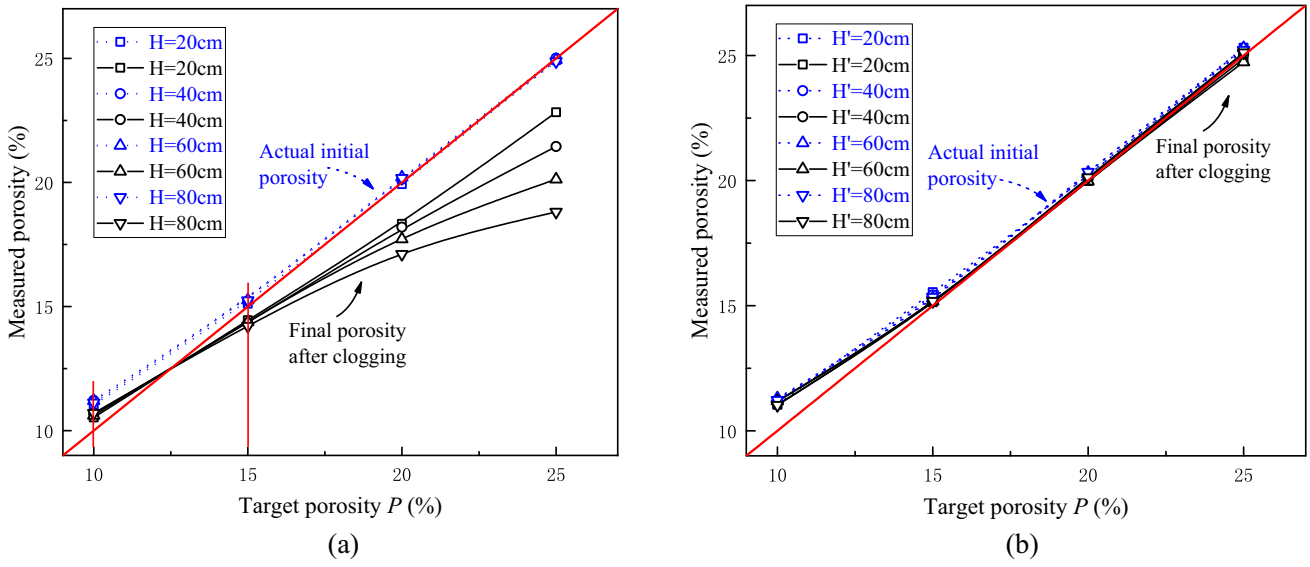

Fig. 16. The relationship between the target porosity and the porosity after clogging. (a) O-PCP; (b) AC-PCP.

and reliable. For the same initial porosity, larger the sampling depth, smaller the final porosity. When the target porosity exceeds 15%, the clogging effect of soil on pervious concrete is visibly increased. In contrast, when the target porosity is less than 15%, the clogging effect of soil on pervious concrete is not very obvious. The final porosity after clogging of AC-PCP is close to the actual initial porosity, which proves that the geotextile has a good anti-clogging effect.

4.3. Excess pore water pressure

The evolution of excess pore water pressure is shown in Fig. 17. The excess pore water pressure increases with increasing burial depth. With this increase, the effect of O-PCP and AC-PCP on the dissipation of excess pore water pressure becomes more obvious. The test data show that excess pore water pressure dissipates faster during 0–20 h. After 20 h, the dissipating rate of excess pore water pressure slowed significantly. Results also show that during the fast dissipating phase, there is no significant change in the dissipation rate for AC-PCP around which non-woven geotextile is employed. This is because the geotextile blocks the soil outside the pile, ensuring the drainage path of the pile.

The relationship between the target porosity and pore water pressure dissipation time are shown in Fig. 18. It can be seen that with an increase in the target porosity, the dissipating time of the excess pore water pressure at each measurement point becomes shorter. With an increase in burial depth, the dissipating time of excess pore water pressure at each measurement becomes longer. When the burial depth is 25 cm and 50 cm, there is little difference between the AC-PCP and O-PCP for excess pore water pressure dissipation. However, when the burial depth is 75 cm, the dissipating time for the AC-PCP composite foundation is significantly reduced compared to O-PCP. This shows that AC-PCP can dissipate higher excess pore water pressure better and once again prove that the geotextile plays a positive role in the prevention of clogging. The PCP length in actual engineering is 10000 ~ 15000 mm while the model was 1000 mm long. Therefore, in practice, the role of the AC-PCP in rapidly dissipating excess pore water pressure could be more significant.

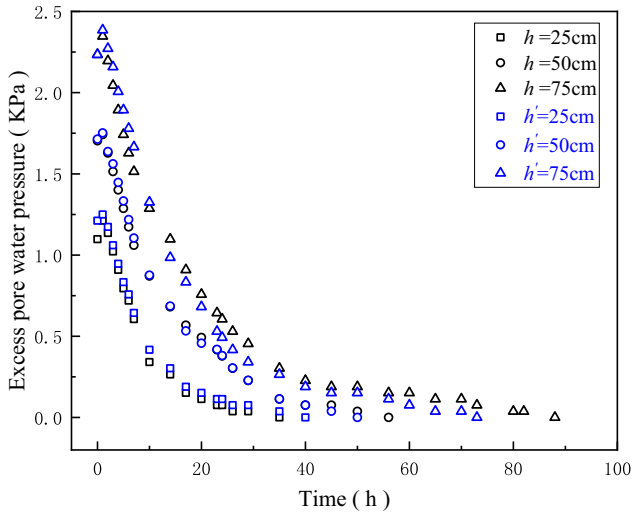

(a) The target porosity of 10%

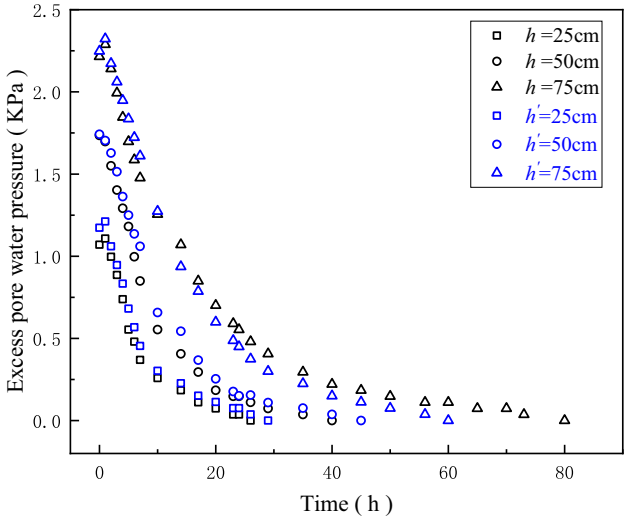

(b) The target porosity of 15%

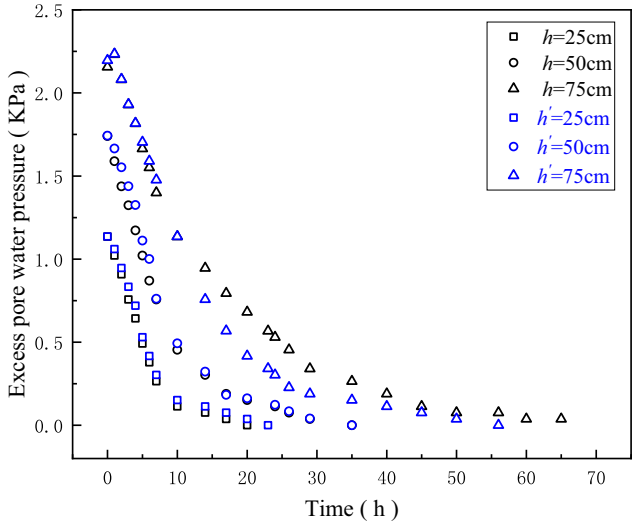

(c) The target porosity of 20%

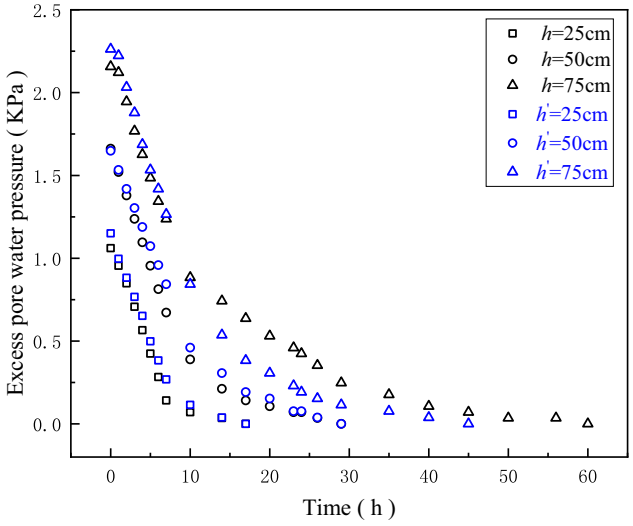

(d) The target porosity of 25%

Fig. 17. Evolution of excess pore water pressure. (a) The target porosity of 10%; (b) The target porosity of 15%; (c) The target porosity of 20%; (d) The target porosity of 25%

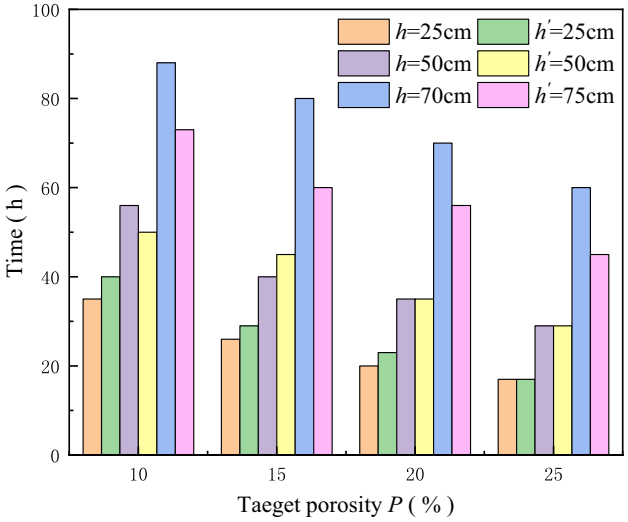

Fig. 18. The relationship between target porosity and pore water pressure dissipation time.

5. Discussion

It should be noted that hydraulic conductivity can be influenced by the porosity, especially the size and distribution of the intercommunicating voids in the PCP. Generally speaking, the hydraulic conductivity increases with porosity [13,17]. However, the voids of pervious concrete are ineffective for seepage because pores have closed entrance or exit even if the voids are large. The actual initial porosity (P_a) and final porosity (P_f) after clogging of PCP were obtained in this study, but these porosities are not intercommunicated porosity. Such porosity would result in a high overestimation of hydraulic conductivity for the PCP. The 3D intercommunicated porosity is generally smaller than this porosity, which is proven by the comparison of numerical and test results [18,24]. The PCP after clogging is still permeable, and the voids' size and distribution of clogging soil and pervious concrete are significantly different. Hence coupling permeability of clogging soils and pervious concrete is more complicated. Further studies on the size and distribution of the intercommunicating voids of PCP based on CT imaging are worthwhile.

6. Conclusion

To study the clogging behavior of PCP caused by the vibrating-sinking tube method and the new anti-clogging PCP performance based on geotextiles, a series of experimental and X-ray CT image analyses were carried out using a physical model system. The following conclusions were drawn:

(1) As the target porosity and sampling depth increase, the degree of O-PCP clogging nonlinearly increases, and the AC-PCP has almost no clogging, which proves that the geotextile shows a good anti-clogging effect. Based on the test results, a preliminary O-PCP clogging model based on the vibrating-sinking tube method is proposed. This model is useful to approximately estimate the clogging depth of O-PCP.

(2) The actual porosity is only slightly higher than the target porosity, indicating that the PCP mix ratio design method and vibrating-sinking tube method process used in this study are accurate and reliable. 15% (target porosity) is a critical value, so in practical engineering, the target porosity design value of O-PCP should not be greater than 15%.

(3) Both O-PCP and AC-PCP can reduce the excess pore water pressure in the ground induced by the vibrating-sinking tube method. However, with an increase in burial depth, the effect of AC-PCP on excess pore water pressure dissipation becomes more obvious, which proves the AC-PCP has a stronger ability to dissipate higher excess pore water pressure. Therefore, compared to O-PCP, AC-PCP can effectively mitigate the liquefaction of soil in composite foundations for a long time.

CRediT authorship contribution statement

Xinzhuang Cui: Conceptualization, Methodology, Resources. **Xiaoning Zhang:** Data curation, Writing - original draft. **Jipeng Wang:** Validation, Investigation, Writing - review & editing. **Jiong Zhang:** Supervision, Software. **Q. Hui:** . **Jun Li:** Formal analysis.

Declaration of Competing Interest

The authors declare that they have no known competing financial interests or personal relationships that could have appeared to influence the work reported in this paper.

Acknowledgments

This work is supported by the National Key Research and Development Project of China (No. 2018YFB1600100), the Natural Science Foundations of China (No. 51778346), and the Key Research and Development Project of Shandong Province of China (No. 2019GSF111007).

References

[1] P. Ariyarathne, D.S. Liyanapathirana, C.J. Leo, Comparison of different two-dimensional idealizations for a geosynthetic-reinforced pile-supported embankment, Int. J. Geomech. 13 (2013) 754–768, https://doi.org/10.1061/(ASCE)GM.1943-5622.0000266.
[2] S. Haldar, G.L.S. Babu, Failure mechanisms of pile foundations in liquefiable soil: Parametric study, Int. J. Geomech. 10 (2010) 74–84, https://doi.org/10.1061/(ASCE)1532-3641(2010)10:2(74).
[3] J.M.O. Hughes, N.J. Withers, Reinforcing of Soft Cohesive Soils with Stone Columns, Gr. Eng. 11 (1974) 234, https://doi.org/10.1016/0148-9062(74)90643-3.
[4] H.B. Poorooshasb, G.G. Meyerhof, Analysis of behavior of stone columns and lime columns, Comput. Geotech. 20 (1997) 47–70, https://doi.org/10.1016/S0266-352X(96)00013-4.
[5] J.S. Lee, G.N. Pande, Analysis of stone-column reinforced foundations, Int. J. Numer. Anal. Methods Geomech. 22 (1998) 1001–1020, https://doi.org/10.1002/(SICI)1096-9853(199812)22:12<1001::AID-NAG955>3.0.CO;2-I.
[6] A.P.F. Pinto, J.D. Rodrigues, Stone consolidation: The role of treatment procedures, J. Cult. Herit. 9 (2008) 38–53, https://doi.org/10.1016/j.culher.2007.06.004.
[7] Z. Guetif, M. Bouassida, J.M. Debats, Improved soft clay characteristics due to stone column installation, Comput. Geotech. 34 (2007) 104–111, https://doi.org/10.1016/j.compgeo.2006.09.008.
[8] J.J. Zheng, S.W. Abusharar, X.Z. Wang, Three-dimensional nonlinear finite element modeling of composite foundation formed by CFG-lime piles, Comput. Geotech. 35 (2008) 637–643, https://doi.org/10.1016/j.compgeo.2007.10.002.
[9] F. Sariosseiri, B. Muhunthan, Effect of cement treatment on geotechnical properties of some Washington State soils, Eng. Geol. 104 (2009) 119–125, https://doi.org/10.1016/j.enggeo.2008.09.003.
[10] B. Le Hello, P. Villard, Embankments reinforced by piles and geosynthetics-Numerical and experimental studies dealing with the transfer of load on the soil embankment, Eng. Geol. 106 (2009) 78–91, https://doi.org/10.1016/j.enggeo.2009.03.001.
[11] J.Q. Jia H.T. Wang J. Li X. Zhang X.G. Fan Analysis of bearing capability of CFG pile composite foundation Chongqing Daxue Xuebao/Journal Chongqing Univ. 34 2011 117–120,127
[12] M.T. Suleiman A. Raich M. O'Loughlin P.C. Piles A.I.G.I. Alternative in: Proc. NSF Eng 2011 Res Innov. Conf. Georg. 2011
[13] V. Marzulli, F. Cafaro, M. Ziccarelli, Hydraulic characterization of a pervious concrete for deep draining trenches, J. Mater. Civ. Eng. 30 (2018), https://doi.org/10.1061/(ASCE)MT.1943-5533.0002274.
[14] P.D. Tennis, M.L. Leming, D.J. Akers, Pervious Concrete Pavements, EB302, Portland Cement Association, Skokie, Illinois, and National Ready Mixed Concrete Association, Silver Spring, Maryland, 2004.
[15] J.D. Luck S.R. Workman S.F. Higgins Hydrologic properties of pervious concrete Trans. ASABE. 49 2006 1807 1813 https://doi.org/10.13031/2013.21029
[16] S. Dean, F. Montes, S. Valavala, L. Haselbach, A New Test Method for Porosity Measurements of Portland Cement Pervious Concrete, J. ASTM Int. (2005), https://doi.org/10.1520/jai12931.
[17] X. Cui, J. Zhang, D. Huang, Z. Liu, F. Hou, S. Cui, L. Zhang, Z. Wang, Experimental study on the relationship between permeability and strength of pervious concrete, J. Mater. Civ. Eng. 29 (2017) 1–9, https://doi.org/10.1061/(ASCE)MT.1943-5533.0002058.
[18] M. Ziccarelli, C. Valore, Hydraulic conductivity and strength of pervious concrete for deep trench drains, Geomech. Energy Environ. 18 (2019) 41–55, https://doi.org/10.1016/j.gete.2018.09.001.
[19] W. Schlüter, C. Jefferies, Modelling the outflow from a porous pavement, Urban Water. 4 (2002) 245–253, https://doi.org/10.1016/S1462-0758(01)00065-6.
[20] J. Zhang, X.Z. Cui, D. Huang, Q. Jin, J.J. Lou, W.Z. Tang, Numerical simulation of consolidation settlement of pervious concrete pile composite foundation under road embankment, Int. J. Geomech. 16 (2016) 1–10, https://doi.org/10.1061/(ASCE)GM.1943-5622.0000542.
[21] M.T. Suleiman, L. Ni, A. Raich, Development of pervious concrete pile ground-improvement alternative and behavior under vertical loading, J. Geotech. Geoenvironmental Eng. 140 (2014) 1–13, https://doi.org/10.1061/(ASCE)GT.1943-5606.0001135.
[22] L. Ni, M.T. Suleiman, A. Raich, Behavior and soil-structure interaction of pervious concrete ground-improvement piles under lateral loading, J. Geotech. Geoenvironmental Eng. 142 (2016) 1–11, https://doi.org/10.1061/(ASCE)GT.1943-5606.0001393.
[23] J. Zhang, G.D. Ma, Z.X. Dai, R.P. Ming, X.Z. Cui, R. She, Numerical study on pore clogging mechanism in pervious pavements, J. Hydrol. 565 (2018) 589–598, https://doi.org/10.1016/j.jhydrol.2018.08.072.
[24] J. Zhang, G.D. Ma, R.P. Ming, X.Z. Cui, L. Li, H.N. Xu, Numerical study on seepage flow in pervious concrete based on 3D CT imaging, Constr. Build. Mater. 161 (2018) 468–478, https://doi.org/10.1016/j.conbuildmat.2017.11.149.
[25] X.Z. Cui, J. Zhang, D. Chen, S. Li, Q. Jin, Y. Zheng, S. Cui, Clogging of pervious concrete pile caused by soil piping: an approximate experimental study, Can. Geotech. J. 55 (2018) 999–1015, https://doi.org/10.1139/cgj-2017-0238.
[26] B. Rehder, K. Banh, N. Neithalath, Fracture behavior of pervious concretes: The effects of pore structure and fibers, Eng. Fract. Mech. 118 (2014) 1–16, https://doi.org/10.1016/j.engfracmech.2014.01.015.
[27] M.S. Sumanasooriya, N. Neithalath, Stereology- and Morphology-Based Pore Structure Descriptors of Enhanced Porosity (Pervious) Concretes, ACI Mater. J. 106 (2009) 429–438.
[28] M.S. Sumanasooriya, D.P. Bentz, N. Neithalath, Planar Image-Based Reconstruction of Pervious Concrete Pore Structure and Permeability Prediction, ACI Mater. J. 107 (2010) 413–421.
[29] X. Kuang, J. Sansalone, G. Ying, V. Ranieri, Pore-structure models of hydraulic conductivity for permeable pavement, J. Hydrol. 399 (2011) 148–157, https://doi.org/10.1016/j.jhydrol.2010.11.024.
[30] S.Y. Chung, T.S. Han, S.Y. Kim, T.H. Lee, Investigation of the permeability of porous concrete reconstructed using probabilistic description methods, Constr. Build. Mater. 66 (2014) 760–770, https://doi.org/10.1016/j.conbuildmat.2014.06.013.

[31] H. Xu, W. Guo, Y. Tan, Permeability of asphalt mixtures exposed to freeze-thaw cycles, Cold Reg. Sci. Technol. 123 (2016) 99–106, https://doi.org/10.1016/j.coldregions.2015.12.001.
[32] X.Z. Cui, J. Zhang, N. Zhang, Z. Gao, W. Sui, C. Wang, Improvement of Permeability Measurement Precision of Pervious Concrete, J. Test. Eval. 43 (2015) 812–819, https://doi.org/10.1520/JTE20130176.
[33] Kishida Hideaki Characteristics Of Liquefied Sands During Mino-Owari Tohnankai And Fufui Earthquakes Soils Found. 9 1969 75 92 http://www.mendeley.com/research/geology-volcanic-history-eruptive-style-yakedake-volcano-group-central-japan.